Bulgarian Journal of Physics vol. **46** (2019) 269–280

On Shape Coexistence and Shape Isomerism in Even-Even Nuclei in the Vicinity of ^{208}Pb

K. Pomorski[1], **B. Nerlo-Pomorska**[1], **J. Bartel**[2], **H. Molique**[2]
[1]Institute of Physics, Theoretical Physics Department, Maria Curie Skłodowska University, Lublin, Poland
[2]Institute Pluridisciplinaire Hubert Curien, Université de Strasbourg, Strasbourg, France

Received *7 November 2019*

Abstract. Extended macroscopic-microscopic calculations of the potential-energy surfaces (PES) in a 4D Fourier deformation-parameter space have been performed for $^{170-204}$Pt, $^{172-218}$Hg, and $^{174-220}$Pb isotopes. Several local minima in the PES corresponding to the ground-state and shape isomers were found. Axial and non-axial electric quadrupole moments as well as moments of inertia were evaluated in these minima.

KEY WORDS: Mac-mic model, shape isomers, electric multipole moments, moments of inertia.

1 Introduction

To use a reliable approach to describe the many facets of nuclear structure requires above all two things: a model that allows to determine the energy of the nuclear system and that is rooted in one way or another in the underlying nuclear force that holds this many-body system together, and on the other hand, an efficient way to describe the huge variety of shapes which that nuclear system can adopt. Without even speaking about extreme deformations like those encountered in the fission process, the multitude of different shapes a nucleus can adopt and which are largely determined by the nuclear quantum shell structure and pairing correlations, but also by such more macroscopic phenomena, like the surface tension or the Coulomb repulsion between protons, have been an ever lasting challenge to the nuclear-physics community. There exist nowadays very performant microscopic approaches like the selfconsistent Hartree-Fock-Bogolubov approximation, the relativistic mean-field theory or ab inito Brueckner calculations which describe the properties of nuclei very well. We believe, however, that nuclear-structure calculations rooted in a macroscopic-microscopic approach and relying on a highly performant macroscopic model together with an efficient way of taking quantum effects into account, has still

its entitlement, not because of arguments regarding computer time, but because of its capacity to reveal more clearly physical effects that sometimes are hidden in extensive numerical treatments. In the present investigation we have adopted such an approach, relying on the Lublin-Strasbourg Drop (LSD) [1] which has proven to be among the very best liquid-drop type models, having, for ground-state masses (2766 nuclei considered), an r.m.s. deviation of less than 0.7 MeV, but also able to account for fission-barrier heights (considering all measured barriers for nuclei with $A \geq 75$) with a good accuracy [1,2]. Quantum effects are taken into account through the Strutinsky shell-correction method [3,4] and pairing correlations in the BCS approach with an approximative projection on the desired particle number [4,5]. To be able to account in a most flexible way for the variety of shapes that a nucleus can adopt, we are using the Fourier shape parametrization [6,7] which is able, with only 4 deformation parameters, to describe the large variety of nuclear shapes from the oblate side up to the extreme prolate elongated and/or necked-in deformations that occur in the fission process [8]. This parametrization is going to be presented in the following section.

2 Fourier Expansion of Nuclear Shapes

Many parametrizations of nuclear shapes starting from Lord Rayleigh's expansion of the nuclear radius $R(\theta,\varphi)$ in spherical harmonics [9], still frequently used nowadays, have been proposed in the past. Some of the most successful are the so-called "*Funny Hills*" shapes [10] of Brack and coworkers and the Trentalange-Koonin-Sierk expansion [11], but many of these require sometimes a prohibitive amount of deformation parameters (degrees of freedom) or represent closed expressions that do not allow to test their convergence. The Fourier expansion that we have proposed recently [6,7] has proven to be rapidly converging and to allow for an accurate description of deformed nuclear shapes [12]. It is given in the cylindrical coordinates by

$$\frac{\rho_s^2(z)}{R_0^2} = \sum_{n=1}^{\infty} \left[a_{2n} \cos\left(\frac{(2n-1)\pi}{2} \frac{z-z_{sh}}{z_0} \right) + a_{2n+1} \sin\left(\frac{2n\pi}{2} \frac{z-z_{sh}}{z_0} \right) \right], \quad (1)$$

where ρ_s is the distance from the z-axis to the surface and R_0 is the radius of the corresponding spherical shape having the same volume, while $2z_0$ is the length of the deformed nucleus with respect to the z-axis. z_{sh} guarantees that the center of the nucleus is located at the origin of the coordinate system. The volume conservation of the deformed nucleus and the mass-center condition yield the following relations:

$$z_0 = \frac{\pi R_0}{3 \sum\limits_{n=1}^{\infty} (-1)^{n-1} \dfrac{a_{2n}}{2n-1}}, \qquad z_{sh} = \frac{3z_0^2}{2\pi R_0} \sum_{n=1}^{\infty} (-1)^n \frac{a_{2n+1}}{n}. \quad (2)$$

Instead of the a_k Fourier coordinates it turns out of great advantage to define through Eq. (3) q_k Fourier coordinates in such a way that, apart from the elongation parameter q_2, which is zero for the spherical shape, vanishing q_k parameters correspond to the LD path to fission and minimize on the average the LD energy

$$\begin{cases} q_2 = a_2^{(0)}/a_2 - a_2/a_2^{(0)} \ , \\ q_3 = a_3 \ , \\ q_4 = a_4 + \sqrt{(q_2/9)^2 + (a_4^{(0)})^2} \ , \\ q_5 = a_5 - (q_2 - 2)a_3/10 \ , \\ q_6 = a_6 - \sqrt{(q_2/100)^2 + (a_6^{(0)})^2} \ , \end{cases} \tag{3}$$

where, $a_{2n}^{(0)} = (-1)^{n-1} \dfrac{32}{\pi^3 \, (2n-1)^3}$ are the expansion coefficients of a sphere. Nonaxial shapes are obtained by assuming that all cross-sections perpendicular to the z-axis have an elliptic form with half-axis a and b, thus defining a non-axiality parameter

$$\eta = \frac{b-a}{a+b} \ , \tag{4}$$

where one assumes, in addition, that $\rho_s^2(z) = a(z)b(z)$ in order to guarantee volume conservation.

One has to mention here that the above description of nonaxial deformations is extremely simple. One could, of course, also expand the shape of the cross-section perpendicular to the z-axis into a Fourier series similar to Eq. (1), but such an attempt would complicate unduly our shape definition.

3 Results

From the long list of stationary points found in our 4-dimensional deformation space, corresponding either to the ground state or to shape isomeric states in the isotopes of platinum, mercury and lead nuclei and which are given in the table below, let us just take the nucleus ^{182}Hg as one illustrative example to make the reader better understand how to look at the deformation-energy landscapes obtained in our Fourier shape parametrization in order to locate and identify shape isomers. To this purpose we show in Figure 1 the energy of that nucleus (relative to the LSD energy of the spherical drop) as projected onto the (q_2, η), the (q_2, q_3) and the (q_2, q_4) planes thus testing respectively, as function of the elongation (quadrupole) q_2 coordinate, the non-axiality η, the left-right asymmetry q_3 (octupole) and the neck q_4 (hexadecapole) degrees of freedom. All three of these figures have been obtained by a minimisation with respect to the two other degrees of freedom. An energy landscape in the (q_2, η) plane, as on top of Figure 1, thus shows the energy of the here studied nuclear system as function of q_2

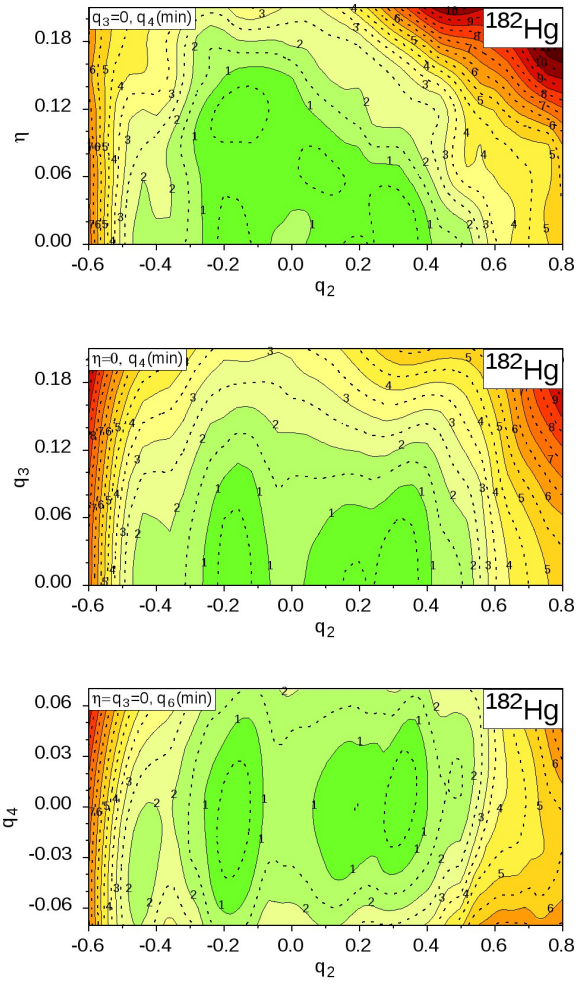

Figure 1. Projections of the 4D deformation-energy surface of ^{182}Hg onto the (q_2, η) (top), (q_2, q_3) (middle), and (q_2, q_4) (bottom) planes.

and η, where in every (q_2, η) deformation point the energy has been minimized with respect to the left-right asymmetry parameter q_3 and the neck degree of freedom q_4.

In the top part of Figure 1 one identifies two axially symmetric ($\eta = 0$) local minima and two local minima that do not correspond to an axially symmetric shape ($\eta \neq 0$), but are, in fact, nothing but the *mirror images* (corresponding simply to a reordering of the coordinate axis) of the axially symmetric oblate and

prolate minima. It has, indeed, to be observed that deformations in the (q_2, η) space obey similar symmetry rules as the ones in the traditional (β, γ) plane (see Ref. [7] for a detailed discussion of this point). This indicates that there are simply no local minima in this nucleus that break axial symmetry. In the (q_2, q_3) plane (middle part of Figure 1) one observes three local minima that are all reflection symmetric ($q_3 = 0$) at q_2= -0.17, 0.18, and 0.32. Since all of them have similar energies, one could speak here about shape-coexistence. Another two minima corresponding to well deformed shapes are observed in the (q_2, q_4) plane (bottom part of Figure 1). An oblate minimum appears at $q_2 = -0.43$ at

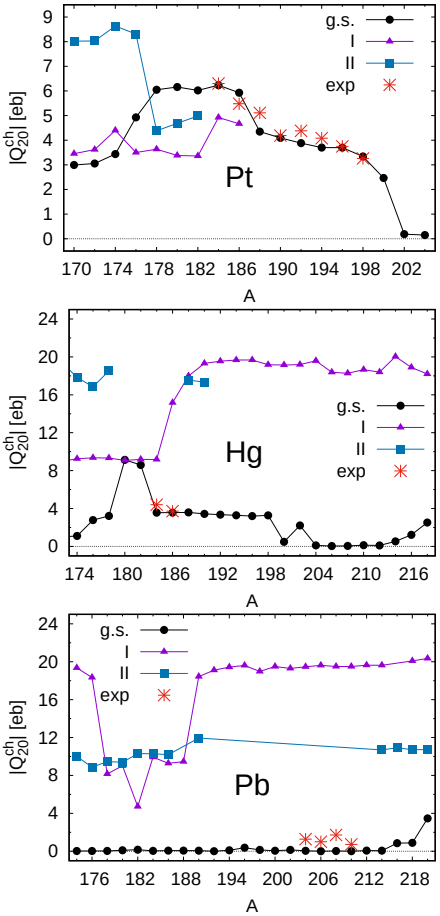

Figure 2. Electric charge quadrupole moments in the ground-state (g.s.) and the two lowest-energy shape isomers (I and II) for Pt (top), Hg (middle), and Pb (bottom) isotopes. The experimental data taken from Ref. [14] are marked by stars.

an energy $\Delta E = 1.58$ MeV above the ground state, while a prolate minimum is found at $q_2 = 0.48$ at an energy of 1.25 MeV above the ground state. Both these minima could correspond to shape isomers. The oblate shape-isomeric state is separated from the ground-state by a barrier higher than 0.5 MeV, so, it has a larger chance to be discovered than the prolate ones for which the barrier height is 0.25 MeV only.

It would be rather difficult to bring in the present report maps for all the isotopes investigated here: $^{170-204}$Pt, $^{172-218}$Hg, and $^{174-220}$Pb. We have therefore decided to record in Table 1 some data corresponding to the found local minima that are lowest in energy. We are thus giving in an Appendix at the end of this paper the energies ΔE of these minima relative to the ground-state, the corresponding axial Q_{20} and non-axial Q_{22} charge quadrupole moments, the octupole moments Q_{30}, as well as the three cranking [13] moments of inertia $J_x,\ J_y$, and J_z.

The theoretical electric quadrupole moments are compared in Figure 2 with the existing experimental data. The observed agreement of our estimates with the data in the ground state of the considered nuclei gives some hope that our predictions of the electric moments of shape isomers are indeed reliable.

4 Conclusions

The following conclusions can be drawn from our investigation:

- The macroscopic-microscopic model with the LSD liquid-drop type energy and quantum corrections obtained in a Yukawa-folded mean-field potential reproduces well the equilibrium deformations of all investigated nuclei.
- A 4-dimensional Fourier deformation-parameter space (η, q_2, q_3, q_4) is used to describe the deformation-energy landscapes of these nuclei.
- The role of higher multipolarity deformations q_5 and q_6 is shown to be in practice negligible.
- A substantial number of shape isomers are predicted in Pt, Hg, and Pb nuclei and await experimental confirmation.

Further calculations for isotopes lighter than Pt are planned in the near future.

Acknowledgements

This work has been partly supported by the Polish-French COPIN-IN2P3 collaboration agreement under project numbers 08-131 and 15-149, as well as by the Polish National Science Centre, grant No. 2016/21/B/ST2/01227.

Appendix

Table 1: Energies ΔE (relative to the ground-state), axial (Q_{20}) and non-axial (Q_{22}) quadrupole, and octupole (Q_{30}) electric moments, and cranking moments of inertia J_x, J_y, and J_z in the ground state and the lowest-energy local minima in the PES of $^{170-204}$Pt, $^{172-218}$Hg, and $^{174-220}$Pb isotopes.

Nucleus	ΔE (MeV)	Q_{20} (fm^2)	Q_{22} (fm^2)	Q_{30} (fm^3)	J_x ($\frac{\hbar^2}{\mathrm{MeV}}$)	J_y ($\frac{\hbar^2}{\mathrm{MeV}}$)	J_z ($\frac{\hbar^2}{\mathrm{MeV}}$)
^{170}Pt	0.00	-299	-174	0	9	2	3
	0.04	345	-115	0	6	11	1
	2.83	-802	0	0	29	29	0
	3.96	1707	-170	0	54	62	5
^{172}Pt	0.00	-305	-211	0	11	2	5
	2.46	-803	0	0	30	30	0
^{174}Pt	0.00	440	-120	0	10	16	1
	2.07	-863	-448	0	42	19	14
^{176}Pt	0.00	493	-113	0	12	19	1
	0.05	-350	-259	0	16	3	7
	2.03	-831	0	0	31	31	0
^{178}Pt	0.00	605	0	0	21	21	0
	0.10	-364	-315	0	18	2	10
	0.82	-438	0	0	12	12	0
^{180}Pt	0.00	616	0	0	21	21	0
	0.32	-338	-348	0	18	1	12
	0.83	-469	0	0	14	14	0
^{182}Pt	0.00	602	-55	0	20	23	0
	0.61	-336	-321	0	18	2	12
	0.79	-498	0	0	16	16	0
^{184}Pt	0.00	623	0	0	26	26	0
	0.76	-492	0	0	17	17	0
^{186}Pt	0.00	593	-70	0	38	40	1
	0.29	-467	0	0	15	15	0
	3.94	1685	0	-46	70	70	0
^{188}Pt	0.00	-435	0	0	12	12	0
	0.18	480	-105	0	15	20	1
	4.10	1763	0	0	74	74	0
^{190}Pt	0.00	-409	0	0	10	10	0
	0.11	380	-141	0	8	15	2
	4.71	1776	0	0	79	79	0

Continued on next page

Table 1 – *Continued from previous page*

Nucleus	ΔE (MeV)	Q_{20} (fm^2)	Q_{22} (fm^2)	Q_{30} (fm^3)	J_x ($\frac{\hbar^2}{\mathrm{MeV}}$)	J_y ($\frac{\hbar^2}{\mathrm{MeV}}$)	J_z ($\frac{\hbar^2}{\mathrm{MeV}}$)
^{192}Pt	0.00	-388	0	0	9	9	0
	5.46	1807	0	0	82	82	0
^{194}Pt	0.00	-370	0	0	9	9	0
	6.80	1741	0	0	81	81	0
^{196}Pt	0.00	-370	0	0	10	10	0
	8.28	1796	0	0	82	82	0
^{198}Pt	0.00	-334	0	0	12	12	0
	8.98	1782	-68	0	81	84	1
^{200}Pt	0.00	-247	0	0	5	5	0
	11.57	1781	-62	0	76	80	1
^{202}Pt	0.00	-19	0	0	0	0	0
	12.99	1857	-107	0	79	86	3
^{204}Pt	0.00	-15	0	0	0	0	0
	14.54	1773	0	0	77	77	0
^{172}Hg	0.00	192	0	-63	3	3	0
	3.76	-898	0	0	32	32	0
	4.46	1949	-52	0	63	65	1
^{174}Hg	0.00	229	0	-60	4	4	0
	3.01	-925	-106	0	44	37	1
	3.70	1784	-123	0	57	62	3
^{176}Hg	0.00	278	0	0	6	6	0
	0.71	797	-71	0	30	34	0
	2.02	-936	0	0	36	36	0
	3.16	1692	-105	0	58	62	2
^{178}Hg	0.00	-322	-63	0	9	6	1
	0.02	287	0	0	6	6	0
	0.08	126	-236	0	0	5	6
	0.49	865	-56	0	42	46	0
	1.59	-932	-0	0	36	36	0
	2.94	1853	-67	0	65	67	1
^{180}Hg	0.00	913	0	0	34	34	0
	0.40	320	0	0	7	7	0
	1.93	-908	0	0	35	35	0
^{182}Hg	0.00	860	0	0	32	32	0
	0.09	-358	0	0	9	9	0
	0.18	173	-242	0	0	8	6
	1.25	1446	0	0	51	51	0
	1.58	-918	0	0	34	34	0

Continued on next page

Table 1 – *Continued from previous page*

Nucleus	ΔE (MeV)	Q_{20} (fm^2)	Q_{22} (fm^2)	Q_{30} (fm^3)	J_x ($\frac{\hbar^2}{\mathrm{MeV}}$)	J_y ($\frac{\hbar^2}{\mathrm{MeV}}$)	J_z ($\frac{\hbar^2}{\mathrm{MeV}}$)
^{184}Hg	0.00	-356	0	0	10	10	0
	0.08	811	0	0	31	31	0
	0.31	440	0	0	15	15	0
	1.72	-918	0	0	34	34	0
^{186}Hg	0.00	-356	0	0	10	10	0
	0.44	333	0	0	9	9	0
	0.44	804	0	0	32	32	0
	2.37	1517	0	0	57	57	0
^{188}Hg	0.00	-359	0	0	10	10	0
	0.50	326	0	0	9	9	0
	3.81	1798	0	0	78	78	0
^{190}Hg	0.00	-343	0	0	9	9	0
	0.46	252	0	0	6	6	0
	4.12	1932	0	0	80	80	0
^{192}Hg	0.00	-335	0	0	8	8	0
	0.57	-121	-127	0	4	0	2
	4.93	1955	0	0	93	93	0
^{194}Hg	0.00	-328	0	0	8	8	0
	5.56	1967	0	0	84	84	0
^{196}Hg	0.00	-320	0	0	8	8	0
	0.62	212	0	0	5	5	0
	7.02	1968	0	0	83	83	0
^{198}Hg	0.00	-327	0	0	10	10	0
	0.71	174	0	0	4	4	0
	8.45	1917	0	0	85	85	0
^{200}Hg	0.00	48	0	0	0	0	0
	0.20	48	0	0	0	0	0
	9.79	1915	0	0	91	91	0
^{202}Hg	0.00	-221	0	0	5	5	0
	11.77	1919	-24	0	85	87	0
^{204}Hg	0.00	11	0	0	0	0	0
	13.81	1959	-62	0	82	86	1
^{206}Hg	0.00	4	0	0	0	0	0
	15.69	1838	0	0	84	84	0
^{208}Hg	0.00	5	0	0	0	0	0
	12.96	1827	0	0	84	84	0
^{210}Hg	0.00	12	0	0	0	0	0
	8.70	-919	0	0	38	38	0
	10.07	1865	0	0	84	84	0

Continued on next page

Table 1 – *Continued from previous page*

Nucleus	ΔE (MeV)	Q_{20} (fm^2)	Q_{22} (fm^2)	Q_{30} (fm^3)	J_x ($\frac{\hbar^2}{\mathrm{MeV}}$)	J_y ($\frac{\hbar^2}{\mathrm{MeV}}$)	J_z ($\frac{\hbar^2}{\mathrm{MeV}}$)
^{212}Hg	0.00	10	0	0	0	0	0
	7.20	-933	0	0	39	39	0
^{214}Hg	0.00	53	0	0	0	0	0
	5.73	2003	0	0	94	94	0
	5.77	-955	0	0	41	41	0
^{216}Hg	0.00	122	-139	0	0	4	3
	4.13	1890	0	0	92	92	0
	4.52	-983	0	0	44	44	0
^{218}Hg	0.00	-252	0	22	6	6	0
	0.25	202	0	282	9	9	0
	3.37	-1042	-405	0	66	36	15
	3.40	1820	0	0	83	83	0
^{174}Pb	0.00	-2	0	0	0	0	0
	4.43	1935	0	0	61	61	0
	4.84	-1001	0	0	39	39	0
^{176}Pb	0.00	-2	0	0	0	0	0
	3.43	1834	53	0	60	58	1
	3.42	-887	-509	0	43	16	15
^{178}Pb	0.00	-3	0	0	0	0	0
	1.46	816	-121	0	28	35	1
	2.26	-945	-522	0	47	19	17
	2.71	1885	0	0	63	63	0
	2.71	-1035	0	0	72	72	0
^{180}Pb	0.00	-10	0	0	0	0	0
	1.60	902	-96	0	42	49	1
	2.13	-940	-524	0	52	21	20
	2.53	-1032	0	0	42	42	0
	2.69	1831	0	0	62	62	0
^{182}Pb	0.00	-16	0	0	0	0	0
	0.39	1050	0	0	38	38	0
	0.45	-472	-630	35	31	1	26
	2.30	-1030	0	0	42	42	0
	4.21	2748	0	0	94	94	0
^{184}Pb	0.00	-4	0	0	0	0	0
	0.76	993	0	0	37	37	0
	2.14	-1029	-35	0	41	40	0
	4.60	2751	0	0	103	103	0
^{186}Pb	0.00	-7	0	0	0	0	0
	1.01	928	0	0	34	34	0
	1.07	228	-300	0	0	11	8
	1.17	-516	0	0	17	17	0
	2.33	-1019	0	0	40	40	0

Continued on next page

Table 1 – *Continued from previous page*

Nucleus	ΔE (MeV)	Q_{20} (fm^2)	Q_{22} (fm^2)	Q_{30} (fm^3)	J_x ($\frac{\hbar^2}{\mathrm{MeV}}$)	J_y ($\frac{\hbar^2}{\mathrm{MeV}}$)	J_z ($\frac{\hbar^2}{\mathrm{MeV}}$)
^{188}Pb	0.00	-7	0	0	0	0	0
	1.33	945	0	0	33	33	0
	2.37	1696	0	0	63	63	0
^{190}Pb	0.00	-6	0	0	0	0	0
	3.19	1843	0	0	73	73	0
	5.77	-1195	-816	0	65	24	29
^{192}Pb	0.00	0	0	0	0	0	0
	3.82	1912	0	0	76	76	0
^{194}Pb	0.00	-10	0	0	0	0	0
	4.79	1943	0	0	82	82	0
^{196}Pb	0.00	38	0	0	0	0	0
	5.26	1961	0	0	83	83	0
^{198}Pb	0.00	-14	0	0	0	0	0
	6.61	1898	0	0	83	83	0
	4.84	-1001	0	0	39	39	0
^{200}Pb	0.00	-5	0	0	0	0	0
	7.96	1950	0	0	85	85	0
^{202}Pb	0.00	-14	0	0	0	0	0
	10.13	1930	0	0	85	85	0
^{204}Pb	0.00	-4	0	43	0	0	0
	11.90	1947	0	0	82	82	0
^{206}Pb	0.00	0	0	0	0	0	0
	13.93	1962	-11	0	80	81	0
^{208}Pb	0.00	-2	0	0	0	0	0
	15.44	1950	0	0	80	80	0
^{210}Pb	0.00	0	0	0	0	0	0
	12.60	1950	0	0	81	81	0
^{212}Pb	0.00	6	0	46	0	0	0
	9.67	1964	0	0	80	80	0
^{214}Pb	0.00	-6	0	0	0	0	0
	0.62	107	0	381	7	7	0
	7.09	1962	0	0	82	82	0
^{216}Pb	0.00	85	0	312	6	6	0
	5.18	2061	0	0	90	90	0
^{218}Pb	0.00	88	0	291	6	6	0
	0.71	-52	0	85	1	1	0
	3.71	2009	0	0	93	93	0
^{220}Pb	0.00	-39	-28	182	2	2	0
	0.46	347	0	0	19	19	0
	2.17	2035	0	0	93	93	0

References

[1] K. Pomorski, J. Dudek (2003) Nuclear liquid-drop model and surface-curvature effects. *Phys. Rev. C* **67** 044316.

[2] A. Dobrowolski, K. Pomorski, and J. Bartel (2007) Fission barriers in a macroscopic-microscopic model. *Phys. Rev. C* **75** 024613.

[3] V.M. Strutinsky (1967) Shell effects in nuclear masses and deformation energies. *Nucl. Phys.* **A95** 420-442.

[4] S.G. Nilsson, C.F. Tsang, A. Sobiczewski, Z. Szymański, S. Wycech, Ch. Gustafson, I.-L. Lamm, P. Möller, B. Nillson, (1961) On the nuclear structure and stability of heavy and superheavy elements". *Nucl. Phys.* **A131** 1-66.

[5] S. Pilat, K. Pomorski, A. Staszczak (1989) New estimate of the pairing coupling constant". *Zeit. Physik* **A332** 259-262.

[6] B. Nerlo-Pomorska, K. Pomorski, J. Bartel, C. Schmitt (2017) Potential Energy Surfaces of Thorium Isotopes in the 4D Fourier Parametrisation". *Acta Phys. Pol.* **B48** 451-454.

[7] C. Schmitt, K. Pomorski, B. Nerlo-Pomorska, J. Bartel (2017) Performance of the Fourier shape parameterization for the fission process. *Phys. Rev. C* **95** 034612.

[8] K. Pomorski, B. Nerlo-Pomorska, J. Bartel, H. Molique (2019) On shape isomers of Pt-Pb isotopes in the 4D Fourier parametrisation. Submitted to *Acta Phys. Pol. B Proc. Supp.*

[9] F.R.S. Lord Rayleigh (1879) On the Capillary Phenomena of Jets, *Proc. Roy. Soc.* **29** 71-97.

[10] M. Brack, J. Damgaard, A.S. Jensen, H.C. Pauli, V.M. Strutinsky, C.Y. Wong (1972) Funny Hills: The shell-correction approach to nuclear shell effects and its applications to the fission process. *Rev. Mod. Phys.* **44** 320-405.

[11] S. Trentalange, S.E. Koonin and A.J. Sierk (1980) Shape parametrization for liquid-drop studies. *Phys. Rev. C* **22** 1159-1167.

[12] K. Pomorski, B. Nerlo-Pomorska, J. Bartel, C. Schmitt (2018) Stability of superheavy nuclei. *Phys. Rev. C* **97** 034319.

[13] S.G. Nilsson, O. Prior (1960) Pair correllations and the rotational moments of inertia of deformed nuclei. *Mat. Fys. Medd. Dan. Vid. Selsk.* vol. **32**, No. 16.

[14] S. Raman, C.H. Malarkey, W.T. Milner, C.W. Nestor, P.H. Stelson (1987) Transition probability, B(E2), from the ground to the first-excited 2+ state of even-even nuclides. *At. Data Nucl. Data Tab.* **36** 1-96.